# Resin-free three-layered Ti/PMMA/Ti sandwich materials: Adhesion and formability study

Melania Reggente, Mohamed Harhash, Sébastien Kriegel, Wenjia He, Patrick Masson, Jacques Faerber, Geneviève Pourroy, Heinz He, Adèle Carrado

# Resin-free three-layered Ti/PMMA/Ti sandwich materials: adhesion and formability study

*Melania Reggente*[*a,b,1], *Mohamed Harhash*[a,c], *Sebastien Kriegel*[b], *Patrick Masson*[b], *Jacques Faerber*[b], *Geneviève Pourroy*[b], *Heinz Palkowski*[*a] *and Adele Carradò*[b]

[a]Clausthal University of Technology, Institute of Metallurgy (IMET), Robert-Koch-Strasse 42, 38678 Clausthal-Zellerfeld, Germany.

[b]Université de Strasbourg, CNRS UMR 7504, Institut de Physique et Chimie des Matériaux de Strasbourg (IPCMS), 23 rue du Loess BP 43, 67034 Strasbourg, France.

[c]Department of Metallurgical and Materials Engineering, Faculty of Petroleum and Mining Engineering, Suez University, P.O. Box 43721, Suez, Egypt.

---

[1] Present Address: Institute of Chemical Sciences and Engineering (ISIC), École Polytechnique Fédérale de Lausanne (EPFL), Station 6, CH-1015 Lausanne, Switzerland

## 1. Introduction

Skull injuries caused by trauma and pathologies, such as tumor, infectious diseases or congenital deformities, may result into serious functional, aesthetical and psychological sequels, requiring the reconstruction of complex craniofacial prostheses. In this field, the choice of suitable biomaterials is the main challenge. Currently, different classes of mono-materials, such as polymers, ceramics and light metals are employed to fabricate skull and mandible prostheses[1]. In particular, poly(methyl methacrylate) (PMMA)[2], polyether ether ketone (PEEK)[3-4], hydroxyapatite (HA)[5–7] and titanium (Ti)[4,6,8] are the most widely used materials in the cranioplasty reconstruction. Ti remains the most widely used metal in biomedical applications due to its biocompatibility[9-11]. In particular, Ti-based plates are generally used to built-up craniofacial prosthesis and replace the bone. As an example, light Ti skull and mandible prostheses are fabricated by using Selective Laser Melting or 3D reconstruction techniques from medical images, which also reduces the possibility of errors during surgery[12-15]. Moreover, PMMA is also extensively used in cranioplasty, due to its biocompatibility, strength, low cost and the possibility of preoperative use[16-17]. On the other hand, these materials are used as materials in food processing where biological aspects have to be taken into account.

However, the mono-materials present many drawbacks, such as inappropriate mechanical properties or their high weight in the case of metals. For medical use, the discrepancy existing between the mechanical properties and the density of the implant and the bone to be replaced results in stress shielding which represents the most limiting factor for a successful substitute[18,19]. Since the mono-materials alone cannot solve this discrepancy in an optimal way, the development of hybrid structures - made of polymers and metals exhibiting new functionalities - can be a suitable approach in many fields of application[20]. Indeed, they take the advantage of

exploiting both the low density and the lightweight, specific of polymers[21], and the high bending resistance and load capacity proper of the metals[20]. Therefore, by combining these two materials, structures possessing new properties, such as high-energy absorption, high corrosion and mechanical resistance coupled with a lightweight, can be fabricated[22]. In particular, layered structures, such as sandwich materials, composed of two metallic skin sheets and a polymer core can be an interesting alternative to design innovative parts[23]. Such sandwich structures are used in the aircraft, automotive and naval industry because of their high acoustic and damping capacity[24-25], high stiffness and strength, good formability and lightweight[20,26–28]. In these systems, an epoxy resin is commonly used as an adhesive agent to stick the polymer core onto the metal skin sheets ensuring good bonding between the two components even under shear load[23]. The toxicity of this adhesive layer[29] evidently prevents their application in the biomedical field and food production. In our previous work[23], it was shown that, following the rule of mixtures, the mechanical properties of the whole sandwich can be tailored according to the skin and core thicknesses (or rather their volume fractions) achieving sandwich configurations with desired properties. In this way, structures with the necessary and designed stiffness and strength can be produced. Moreover, their formability into complex shapes - as required in the fabrication of prostheses or special parts in industry - can be assured by selecting the proper sandwich components, adjusting the skin/core thickness configuration and improving the metal/polymer bonding strength.

Although sandwich structures seem to be well adapted to the mechanical properties required in biomaterials, the use of an epoxy resin is a serious drawback for *in vivo* applications and if being used in the food industry[29]. Thus, in order to extend their applications, the challenge is to establish a strong, biocompatible bonding between metal and polymer to include a polymer

component between two metal sheets without using an epoxy resin able to attenuate stress-shielding effects.

In general, the durability of a polymer-metal interface strongly depends on the adhesion strength between the two components. Since chemical bonds between metal and polymer are not spontaneously established, these layered hybrid polymer-metal materials often exhibit undesired delamination phenomena due to a weak interfacial adhesion between metal and polymer resulting in the premature failure of the entire system[30,31]. Thus, recently grafted polymers (i.e. polymer chains with an extremity covalently bound to a substrate) were proposed as adhesives to be inserted between a metal substrate and a polymer coating [31-35]. In particular, it has been shown that by exploiting the miscibility between the surface-confined polymer chains and those of a bulk[36-40], melt [33] or solution polymer [35], the metal/polymer adhesion strength is enhanced and their durability improved[31,33,35]. Indeed, when two compatible polymers (i.e. polymer of the same nature) enter in intimate contact, a partial interpenetration between the chains of two materials is established, according to the diffusion theory described by the reptation model [39-41], and, as a result, entanglements points are created[37,38]. The degree of interpenetration depends on three main factors: (i) the brushes surface density (i.e. the number of grafted chain per $nm^2$); (ii) the brushes chains length; and (iii) the molecular weight distribution (MWD) [37,38,42,43]. Long chains in the low-density regime (also called as mushroom regime) are required to obtain a good penetration. Since in this regime the overlap between adjacent chains are avoided, they have enough free-volume to move, re-arrange and interpenetrate in the adhering material [37,38]. It has also been demonstrated that higher chain lengths result in an improvement of the adhesiveness between the polymer bulk and the brushes[37]. In particular, an increase of the tensile strength of a junction formed by grafted PMMA chains interpenetrated in a melted PMMA matrix were

reported when longer brushes chains were considered, due to a deeper penetration of the PMMA brushes into the bulk PMMA[33]. Since, it has been demonstrated that brushes with a degree of polymerization (i.e. the ratio between the molecular weight of the grafted chains and the molecular mass of the monomer) greater than or equal to 200 is necessary to establish physical entanglements with the adjacent polymer bulk[37], the optimization of coating methods enabling the production of films with large thicknesses (few micrometres) are desired[44].

In this context, the idea of this work was to employ surface-confined polymers to fabricate biocompatible resin-free sandwich materials by sticking the polymer core on the metallic skins previously coated with grafted polymer chains. As proof of concept for biomedical applications, Ti and PMMA were employed and Ti/PMMA/Ti sandwiches produced. Indeed, despite the significant discrepancy between the mechanical properties of Ti and those of the surrounding tissues, which often results in a stress shielding[9,10]. In order to reduce this tissue-implant mechanical impairment, a technique to incorporate a polymer component to Ti implants was developed and sandwich materials, made of two Ti skins and a PMMA core, were produced using grafted polymer chains as an adhesive. Therefore, surface-confined PMMA chains replaced the epoxy resin layer and the adhesion between these tethered chains and those of an adhering PMMA sheet (used as core material) was established by exploiting their miscibility through the formation of entanglements. In particular, the PMMA chains were grown on alkali-activated Ti surfaces[45] through surface-initiated atom transfer radical polymerization (SI-ATRP)[46] using phosphonic acid derivatives as coupling agents and malononitrile as polymerization activator[47,48]. Being the established graduate structure characterized by a high Ti/PMMA adhesion strength[45], high thickness (i.e. long PMMA chains)[45] and a porous structure (i.e. high free volume)[45,49] the possibility to use these PMMA-coated Ti surfaces for the

production of sandwich is shown here. Indeed, Ti/PMMA/Ti sandwiches were obtained by hot-pressing, exploiting the interpenetration between the grafted PMMA chains and those of an adhering PMMA foil used as core material [31-37]. Moreover, the Ti/PMMA/Ti bonding strength, mechanical properties and forming behaviour were evaluated performing pull-off tests, standard tensile, bending, Erichsen and deep-drawing tests, respectively.

## 2. Experimental

### 2.1 Sample preparation

PMMA foils (0.5 mm thick) containing $BaSO_4$ fillers and Grade 2 Ti sheets of different sizes (20 × 20 × 0.4 $mm^3$, 20 × 60 × 0.4 $mm^3$, 20 × 80 × 0.4 $mm^3$, 20 × 80 × 0.2 $mm^3$, 25 × 100 × 0.4 $mm^3$, 70 × 70 × 0.4 $mm^3$, 105 × 148 × 0.2 $mm^3$) were used. These sizes were chosen with respect of the minimal sized requested by each mechanical test performed (e.g., pull-off, bending, drawing). Before operation, PMMA foils were rinsed several times with ethanol and Ti sheets cleaned by ultrasonication in acetone, ethanol, and deionized water, 10 min each. The solvents were purchased from Carlo Erba.

### 2.2 Grafting of PMMA chains on Ti substrates

PMMA chains were grafted onto Ti substrates using a three steps strategy previously developed [45]. With respect to this methodology, only the grafting conditions were optimized by considerably reducing the treatment time and the initiator concentration. Firstly, Ti surfaces were activated by immersing the Ti sheets for 1h in a 2M sodium hydroxide (NaOH) concentrated aqueous solution heated up to 80°C [45]. Secondly, a synthesized bromoisobutyrate-

undecyl-1-phosphonic acid ($C_{15}H_{30}O_5PBr$) was immobilized on the Ti surfaces using a "grafting from" method performed in a 0.05 M initiator concentrated aqueous solution at 100°C for 3 h; Thirdly, a SI-ATRP was carried out to grow the PMMA chains according to a previously described procedure[45]. The initiator-modified samples were suspended in a flask equipped with a magnetic bar, which was then degassed three times (by alternating vacuum and argon) and finally filled with argon. Reagents were then added to the flask according to the following order and concentrations: [Cu(I)Br]: 14 mM; [PMDETA]: 12 mM; [anisole]: 4.1 M; [malononitrile]: 14 mM; [MMA]: 5.3 M. Whereas, because of the required greater solution volume, A6-sized Ti sheets were treated using the following conditions: Cu(I)Br]: 3 mM; [PMDETA]: 3 mM; [anisole]: 3.7 M; [malononitrile]: 3 mM; [MMA]: 5.3 M. At the end of the polymerization reaction, the samples (hereafter called PMMA-coated Ti) were cleaned for 10 min in an ultrasonic bath containing methanol to remove the untethered polymer as well as the residues of Cu(I)Br and PMDETA.

### 2.3 Chemical characterization of the grafted PMMA layers

After each step of the PMMA-coated Ti synthesis procedure (namely, the alkali treatment, the grafting of the initiator and the polymerization) the chemical properties of samples' surfaces were investigated. In particular, attenuated total reflection Fourier transformed infrared spectroscopy (ATR-FTIR) analysis - performed with a PerkinElmer spectrometer with a resolution of 4 $cm^{-1}$ - was used to scan the surface-exposed chemical groups, whereas, energy dispersive x-ray spectroscopy (EDX) allowed individuating surfaces' elemental composition. This latter analysis was carried out using a Quantax EDX system embedded in a crossBeam®

Workstation AURIGA-Zeiss 405 Microscope. The analysis of the Ti/PMMA/Ti sandwich fracture surfaces after pull-off tests were studied on a Zeiss GeminiSEM 500 SEM fitted with an EDX system from EDAX (Octane Elite SDD detector + TEAM software).

### 2.4 Morphological characterization of the grafted PMMA layers

Scanning electron microscopy (SEM) was employed to follow the evolution of the surface morphology after each steps of the synthesis procedure and to investigate the resulting PMMA-coated Ti cross-section. In particular, the morphology after the alkali activation, the grafting of the initiator and the SI-ATRP reaction was imaged with a crossBeam® Workstation AURIGA-Zeiss 405 Microscope. Instead, the sample's cross-section was firstly prepared using a ion beam cross-polisher (Hitachi IM4000+). The samples were cut with a metallographical saw and an edge from the backside was polished with a 25° bevel (SiC P1000 paper) to reduce the thickness of Ti to polish by the ion beam. The cross polishing was then performed from the back side (6 keV, Ar). By this way, the organic materiel was protected by the Ti itself and very few exposed to the ion beam. Then its features studied using SEM analysis conducted on a Zeiss Gemini SEM 500 SEM.

### 2.5 Ti/PMMA/Ti sandwich production

Resin-free Ti/PMMA/Ti sandwiches of different sizes were produced by hot-pressing. A PMMA foil 0.5 mm thick, used as core material, was inserted between two PMMA-coated Ti sheets. Since the manufacturing process, regarding the bonding properties between metal and polymer, is independent from the thicknesses of the partners, and with the aim of firstly proving the

feasibility of producing suitable resin-free sandwich materials, the combinations tested were chosen depending on the materials available.

A layup of the three components was then hot-pressed together above the PMMA glass transition temperature and melting temperature (111°C and 160°C, respectively). Bonding was achieved by exploiting the interpenetration of the grafted PMMA chains into the chains of the adhering PMMA foil, which led to the formation of entanglements[31,33].

The main parameters involved in the hot-pressing process are time, temperature and pressure. The optimized combinations of these three parameters for the Ti/PMMA/Ti sandwiches production were assessed performing a parametric study. For each parameter, three values were considered as follows: T = 170, 180 and 200°C, t = 30, 60 and 90 min and p = 0.1, 0.2 and 0.4 MPa. Thus, the maximum number of parameter combinations (i.e. possible experiments) was $3^3$, which were reduced to an optimized number of 19 experiments, by using a design of experiments (DoE) tool, namely Minitab (Minitab Inc.). Successively, the best conditions for the sandwich production were chosen as the ones guarantying the highest value of bonding strength, evaluated performing pull-off tests. The optimum was identified with t = 90 min, T = 180°C and p = 0.2 MPa, so, Ti/PMMA/Ti of different sizes were produced under these condition to perform mechanical and forming tests.

### 2.6 Investigation of the Ti/PMMA/Ti cross-section microstructure

The microstructure of the Ti/PMMA/Ti cross-sections were analysed by Optical microscopy. The samples were prepared by cutting, with a shear cutting bank, a small piece (20 × 10 $mm^2$) of a Ti/PMMA/Ti sandwich from an A6-sized one. Then, the cross-section of the samples was

mounted using cold mounting resin and successively prepared for the observation by wet-grinding using SiC papers and polishing it with synthetic polishing fibre cloth with diamond paste (in a sequence of 6, 3 and finally 1 μm). Finally, the polished Ti/PMMA/Ti cross-sections were observed by optical microscopy (Olympus IX70 and Zeiss AxioImager).

### 2.7 Evaluation of the Ti/PMMA/Ti sandwich adhesion: Pull-off tests

The Ti/PMMA/Ti adhesion strength was evaluated performing pull-off tests. For these tests, sandwiches made of two (20 × 20) $mm^2$ Ti skin sheets and a PMMA core 0.5 mm thick were produced using the conditions listed in Table 2, at least three samples each in most of the conditions. A two-components adhesive (3M scotch-weld DP 490 Structural adhesive epoxy) was used to stick their external surfaces onto an (20 × 20 × 100) $mm^3$ stainless steel bar. Before testing, the glue was cured by heating it at 60°C for 24 h, and then it was kept at room temperature for 48 h. The samples were then mounted on the universal testing machine and the tests performed using a speed of 0.1 mm/min.

### 2.8 Evaluation of the Ti/PMMA/Ti sandwich adhesion: Shear-tests

The shear resistance of the Ti/PMMA/TI sandwiches was evaluated performing single shear tests using a universal testing machine with an applied speed of 1 mm/min. Sandwiches of two PMMA-coated Ti sheets (25 × 100 × 0.4 $mm^3$) and a PMMA core foil, 0.5 mm thick, were produced according to the optimum processing conditions. A defined overlapping area of about

275 $mm^2$ (25 × 11 $mm^2$) based on the thickness and the yield strength of the Ti sheets was chosen following ASTM D3165.

### 2.9 Tensile properties of the Ti/PMMA/Ti sandwiches

The mechanical properties of the Ti sheets, PMMA foils as well as the ones of Ti/PMMA/Ti sandwiches made of two PMMA-coated Ti sheets 0.2 mm thick and a PMMA core 0.5 mm thick (here after noted as 0.2/0.5/0.2 sandwiches) were determined by uniaxial tensile testing. According to ASTM E8, tensile samples of Ti and Ti/PMMA/Ti sandwich were prepared. In particular, Ti/PMMA/Ti sandwich samples were cut from an A6-sized sandwich previously produced using the parameter described in section 2.4.1. Whereas, PMMA foils were prepared and tested according to EN ISO 527-3-1B-50.

### 2.10 Forming behaviour of Ti/PMMA/Ti sandwiches

The forming behaviour of Ti/PMMA/Ti sandwiches were analysed performing three-point bending as well as deep drawing and Erichsen tests. These tests allow identifying and correlating the possible failure modes arising from forming such three-layered sandwich materials under different loading conditions. In principle, failure can be expected in the form of: 1) cracking of the outer Ti skin sheet, which is more probable for thin ones; 2) cracking of the core layer, especially if the core has brittle nature; or 3) interlaminar delamination in case of weak skin/core adhesion characteristics. To this purpose, combinations of sandwiches with different Ti size (20

× 60 mm2 and 20 × 80 mm2) and thicknesses (0.2 mm, 0.4 mm) were produced under the obtained optimum conditions. The following symmetric and asymmetric Ti/PMMA/Ti configurations were produced: (i) 0.2/0.5/0.2; (ii) 0.2/0.5/0.4; (iii) 0.4/0.5/0.4.

### 2.10.1 Three-point bending tests

The bending properties of the Ti/PMMA/Ti sandwiches were investigated performing three-point bending tests using punch sizes of 3 mm and 6 mm in diameter. In particular, the 3 mm punch was used to investigate the properties of the 0.2/0.5/0.2 and 0.4/0.5/0.4 sandwiches, while the 6 mm punch was taken for the asymmetric 0.2/0.5/0.4 ones. The test speed was kept constant at 0.3 mm/s.

The performed test strategy was the following: Firstly, the maximum achievable bending angle, defined as the ones at which a visible failure of the systems (listed above) occurred, was determined. Secondly, to follow the development of the bent sandwiches' strains as well as the degree of their springback, stepwise tests were performed using a 45° step sequence. For this, the test was stopped at the specified angle under load, the strain distribution and the springback were evaluated and documented, prior to carrying on the next step. It is noteworthy to mention that the bending angle was controlled by the previously determined bending displacement according to the controlling equation of DIN EN ISO 7438-2005.

The strain field was determined using photogrammetry (GOM Argus) for the different successive steps. For this analysis and for a precise evaluation, fine dot pattern (0.5 mm point diameter with 1 mm distance of the adjacent dot centres) was etched on the Ti sheets by means of an electrolytic marking system (EU-Classic, Östling Marking Systems GmbH). Successively,

a GOM Argus system was used to determine the strains. The results were obtained in terms of the distribution of the major strain in a section along the sample length; in addition, 3D photogrammetric images show the critical regions of the shaped samples.

Whereas, the spring-back ratios (K) are determined based on the angle ratio between the angle after unloading ($\alpha_2$) with respect of the one in the loading condition ($\alpha_1$):

$$\boldsymbol{K = \frac{\alpha_2}{\alpha_1}} \quad (1)$$

A small spring-back is achieved if the K value is close to 1.

The spring-back degree (K) is correlated to elastic modulus in the plane strain condition ($E'$) according to the geometrical and mechanical properties of the tested sheets[50]:

$$\boldsymbol{K = 4\left(\frac{R_i \times YS}{E' \times t}\right)^3 - 3\left(\frac{R_i \times YS}{E' \times t}\right) + 1} \quad (2)$$

where $R_i$ is the initial bend radius before spring-back, t is the sheet thickness, YS is its yield strength.

In (2) $E'$ is expressed as a function of the Poisson ration (??)[51]:

$$\boldsymbol{E' = \frac{E}{1-\nu^2}} \quad (3)$$

According to (2), lower springback (i.e., better angle stability) is expected with lower YS/E ratio as well as lower R/t ratio.

### 2.10.2 Deep-drawing tests

The possibility of shaping forms that are more complex was investigated by testing the forming properties of Ti/PMMA/Ti sandwiches with different thicknesses (0.2/0.5/0.2, 0.4/0.5/0.4 and the asymmetric 0.2/0.5/0.4).

Deep-drawing tests were performed at room temperature (RT) until failure or complete cup drawing using a drawing ratio $ß_0$ = 1.8, i.e., the ratio between the diameters of the blank (60 mm) and punch (33 mm). During the tests, the drawing speed was kept constant at 0.5 mm/s. As the bending tests, deep drawing tests were performed stepwise based on the failure limit of the drawn sandwich samples. At 6.8 mm, no visual cracking of the Ti skin sheets occurred. In this regard, the deep drawing was carried out first until a displacement of 5 mm, progressively followed up to 10 mm displacements. Finally, the complete drawing of the test samples was accomplished. Moreover, for comparison, the drawing properties of Ti sheets of 0.2 mm thickness and those of the PMMA foils with a thickness of 0.5 mm were investigated performing the tests according to the same procedure.

### 2.10.3 Erichsen test

Erichsen tests – giving information on the stretching behaviour of sheet material - were carried out on 0.2/0.5/0.2 Ti/PMMA/Ti sandwiches. A standard 25 mm diameter semi-spherical punch was used. During the test, the punch displacement rate was kept constant at 0.5 mm/s. The forming limits were determined in terms of the corresponding punch displacement when cracking occurs (namely the Erichsen Index (IE)) and forming force could be determined.

## 3. Results

### 3.1 Grafted PMMA layer bounded on Ti surfaces

The cross-section of PMMA chains grafted on a Ti substrate obtained following a three-step strategy[45] is shown in **Figure 1a**. In the first step, a chemical activation of the Ti surfaces in a

basic media was performed to increase the hydroxyl groups' content enabling the phosphonic acid to anchor. This treatment represents the key element of the procedure and led to the formation of a nanostructured porous layer (see the bottom top-view micrograph in **Figure 1b**) the interconnected porosity of which was used as scaffold to drive the following polymerization and to create a further mechanical interlocking between the substrate and the growing PMMA layer. In the second step, the ATRP initiator (2-bromo-2-methyl-propionic acid 11-phosphono-undecyl ester, $C_7H_{14}O_5PBr$) was grafted on the alkali-activated Ti surfaces (see **Figure 1b** in the middle); the anchoring was established by creating covalent Ti-O-P bonds between the surface hydroxyl groups and the phosphonic acid derivative[45,47,48]. Compared to our previous work[45], we could reduce the time of the grafting treatment from 24h to 3h. Indeed, by measuring the pH during the reaction, a plateau was reached after 3h and no more variations were detected. Moreover, the ATRP initiator concentration was decreased to 0.05 M without noticing significant difference in the resulting surfaces previously treated with a ~0.8 M initiator concentration (for a morphological and chemical comparison between a 3h and a 24h $C_7H_{14}O_5PBr$–modified Ti surfaces see **Figure S1** in the supplementary information (SI)). Finally, in the third step, the hybrid PMMA-coated Ti surfaces were obtained by growing the PMMA chains from the initiator-modified Ti surfaces. As highlighted by the SEM micrograph in **Figure 1b** (top) the polymerization reaction results in a rounded PMMA layer covering the entire surface, characterized by an underneath porosity localized at the Ti/PMMA interface (**Figure 1a**)[45,49].

Additionally, the effect of using a shorter ATRP initiator (i.e., a commercial bromoisobutyrate-propyl-1-phosphonic acid, $C_7H_{14}O_5PBr$) on the polymer thickness and structure was investigated. Whereas, a comparison between the surface morphologies before and after the grafting of the

two (different in size) initiator molecules together with the corresponding EDX spectra, is presented in **Figure 2**. The SEM micrographs highlight that the surface features change after the grafting reaction. In particular, the surface, modified with the shorter initiator (**Figure 2b**), was characterized by the organic molecules bounded around the pillars left by alkali-activated Ti surfaces. Thus, it led to a morphology similar to that of the microporous layer (**Figure 2a**) but less branched. Instead, the grafting of the longer initiator results in a more compact structure composed of sharper pillars (**Figure 2c**). Thus, as expected, the longer initiator filled up better the pores left by the alkali treatment. This reorganization of the surfaces was also confirmed by EDX analysis, the spectra of which were used to determine their elemental composition. After the grafting reaction, the absence of the peak pertained to the sodium, visible after the alkali treatment (**Figure 2d**), suggests that the grafting reaction leads to a reorganization of both the surface morphology and composition. Moreover, the organic content (carbon peak at 0.277 keV) increases and the signals related to the bromine (Br), typical of the α-bromo ester group, and that attributed to the phosphorous (P) of the phosphonates appear (**Figure 2d** and **Figure 2e**).

Then, taking into account the difference in the number of mols produced by using shorter molecules, the reagents quantity required for the polymerization was recalculated in function of the initiator's number of mols and the ATRP consequently carried-out. As previously underlined, the grafting reaction with the shorter initiator leads to a more open surface structure, which results in the growth of less densely packed PMMA layers (**Figure 3**). Indeed, it appears highly porous and composed of globules of organic materials preferentially grown around the pillars of the microporous layer. Thus, for the purpose of this work, in order to get longer grafted PMMA chains, - guarantying a better interpenetration into the ones of the adhering PMMA foil, and thus

a stronger bond[28] - the long bromoisobutyrate-undecyl-1-phosphonic acid ATRP initiator was employed.

### 3.2 Production of Ti/PMMA/Ti resin-free sandwiches

Successively, a procedure to stick a 0.5 mm thick PMMA foil between two synthesized PMMA-coated Ti sheets was developed by replacing the epoxy-resin, usually employed in the fabrication of sandwich materials, with the previously grown tethered polymer chains. Thus, resin-free Ti/PMMA/Ti sandwiches were produced by hot-pressing. The best possible experimental conditions for the Ti/PMMA/Ti sandwiches production were assessed performing a parametric study using a design of experiments (DoE) method, adopting Minitab Inc. as tool for the data analysis. In particular, in order to reduce the number of the experiments to be performed, an optimal factorial DoE plan was applied by hypothesizing that the simultaneous interaction of the three parameters involved in the production (i.e. temperature, time and pressure) is negligible. In this way, 19 experimental combinations (listed in **Table 1**) were selected and Ti/PMMA/Ti sandwiches were accordingly produced.

Then, the corresponding Ti/PMMA adhesion strength was evaluated performing pull-off tests using (20 × 20) $mm^2$ sandwich samples. The optimum conditions for the sandwich production were chosen as the ones guarantying the highest value of the bonding strength according to the data reported in Table 1 and the graphical representation in **Figure 4**. This latter shows the correlation between hot-pressing time and temperature at a constant pressure of 0.1 MPa (**Figure 4a**), 0.2 MPa (**Figure 4b**) and 0.4 MPa (**Figure 4c**), respectively. In general, it can be stated that by increasing the hot-pressing time and/or the temperature, the pull-off strength improves. When a pressure of 0.1 MPa is applied (see **Figure 4a**), the maximum possible pull-off strength can be

reached only at higher temperatures (200°C), which is not recommended to be used. Indeed, it should be considered that the processing temperature should not overstep or even come close to the degradation temperature of the PMMA foil (~205 °C see **Figure SI.2**), especially in case of long hot-pressing times. On the other side, by increasing the pressure to 0.4 MPa, the time required to reach the maximum pull-off strength is reduced, however, the temperature should be still above 195 °C to deliver high strengths (see **Figure 4c**). Moreover, the high pressure led to a squeeze-out of the PMMA core and/or the possible onset of the PMMA degradation, which can lead to undesired thickness inhomogeneities. Whereas, by applying a pressure of 0.2 MPa, the maximum pull-off strength can be reached at an average temperature of 180 °C and a time more than 80 min (see **Figure 4b**). In this work, we selected the following process conditions: temperature T = 180 °C, time t = 90 min and pressure p = 0.2 MPa, which ensure the highest possible pull-off strength (24 MPa) avoiding a squeezing-out and degradation of the polymer.

### 3.3 Evaluation of the Ti/PMMA/Ti adhesion strength

The pull-off tests performed (as sketched in **Figure 5a**) on three Ti/PMMA/Ti sandwiches produced using the optimized conditions led to the results shown in **Figure 5b**. In particular, two samples (Ti/PMMA/$Ti_1$ and Ti/PMMA/$Ti_3$) broke within the glue used to mount the sample to the steel support (see **Figure 5a**) indicating that the Ti/PMMA adhesion strength is higher than that of the Ti/steel glue. Whereas, in the last sample (Ti/PMMA/Ti-$_2$) failure occurred within the PMMA sheet (at  24 MPa).

Moreover, the Ti/PMMA/Ti failure mechanism was identified by analysing the morphology and the chemical composition of the sandwich fracture surfaces after the pull-off tests (a representative image of which is shown in **Figure 5c**), by using SEM-EDX measurements. The

EDX elemental analysis and the SEM micrographs of the PMMA foil (**Figure 5e**) - used as core material - showed that it contains $BaSO_4$ fillers (white spots in **Figure 5e**). Since traces of $BaSO_4$ particles were found also in the Ti/PMMA/Ti surface fracture (SF) (see **Figure 5c** and EDX spectra in **Figure 5d**), we concluded that the fracture occurred within the PMMA core and consequently the failure mechanism is of cohesive nature. Additionally, the shear resistances of the sandwiches were evaluated performing single shear tests on Ti/PMMA/Ti samples as schematized in **Figure 6a**. Two metal sheets (schematized in black in **Figure 6a**) were inserted between the sample and the jaws of the tensile machine in order to ensure the axiality and avoid bending phenomena during the tests.

The results of three representative Ti/PMMA/Ti sandwiches are shown in **Figure 6b**. It can be pointed out that failure occurred within the PMMA foil (see the surface fracture in **Figure 6c**) for ultimate shear strength of (10 ± 2) MPa. For comparison, the shear resistance of three sandwiches composed of two brushed Ti sheet skins (0.4 mm thick) and a PMMA foil with a thickness of 0.5 mm were also investigated. The average Ti surface roughness after the brushing treatment was found equal to (2.7 ± 0.3) µm, almost five times higher than those of the untreated ones (0.5 ± 0.1) µm. The results allowed evaluating a Ti/PMMA bonding strength of (0.9 ± 0.1) MPa, which is much lower than those obtained using the PMMA-coated Ti samples. The weak Ti/PMMA adhesion strength is totally due to (the only) mechanical interlocking of the PMMA into the irregularities of the Ti surfaces since no chemical treatment was performed on the metal sheets and also due to the inertness behaviour of the PMMA, which possesses a low adhesiveness nature.

### 3.4 A6-sized Ti/PMMA/Ti sandwiches: scale-up of the fabrication process

In order to investigate both the mechanical properties and the forming behaviour of Ti/PMMA/Ti sandwiches, A6-sized Ti sheets (105 × 148) $mm^2$ × 0.2 mm thick, were coated with grafted PMMA chains by employing a larger volume of solution (~ 1000 ml) contained in a bigger reactor. Despite a thicker PMMA layer was obtained in the part of the Ti sheet closer to the magnetic stirrer (due to an unsteady mixing of the reagents), the entire surface was completely covered (see **Figure S3** in SI). Then, A6-sized Ti/PMMA/Ti sandwiches were produced by hot-pressing (see **Figure 7a**), as previously explained, using a 0.5 mm thick PMMA foil as core material. The resulting sandwich cross-section, obtained by cutting a A6-sized sandwich, was analysed by optical microscopy and the corresponding image is displayed in **Figure 7b**.

### 3.5 Mechanical properties of Ti/PMMA/Ti sandwiches

In order to study the mechanical properties of this system as well as the ones of Ti sheets and PMMA foils mono-materials, mini-tensile samples of Ti and Ti/PMMA/Ti sandwiches were prepared, according to ASTM E8. PMMA samples were prepared and tested according to EN ISO 527-3-1B-50. The results of the tensile tests are given in **Figure 8.** As expected, the Ti sheets (black curves) exhibit the highest strength values with a Young's modulus of 108 GPa and an ultimate tensile strength (UTS) of 441 MPa as well as a strain at failure of 27% (see **Table 2**), while the PMMA foil shows a brittle behaviour (blue curves). Stiffness and UTSs values of the samples are listed in **Table 2**.

The brittleness of the PMMA is expected to influence the stress-strain behaviour of the entire sandwich sheets under tensile loading as well as the forming behaviour under bending and deep-drawing loading conditions. In this regard, it was observed that the PMMA core cracks earlier

than the pure Ti skin sheets in the sandwich (in strain range between 22% and 28%, red curves) with a strain difference of about 2% at the end of the tensile testing (see black arrows in **Figure 8**). Nevertheless, the total elongation of the Ti/PMMA/Ti sandwiches failures comes close to that ones of the Ti sheets. It is noteworthy to mention that even if there was a slight strain difference between the Ti and PMMA inside the sandwich sheet, no delamination failure could be stated.

Furthermore, using the RoM[23] (Eq. (1)) the Young's modulus of the sandwich ($E_{SMs}$) can be predicted using the PMMA (EPMMA) and Ti sheets ($E_{Ti}$) Young's moduli combined with their volume fraction ($f_{PMMA}$ and $f_{Ti}$, respectively), as follows:

$$E_{SMs} = f_{PMMA}E_{PMMA} + f_{Ti}E_{Ti}$$

As stated before[23], depending on the thickness ratio of the mono-materials, it is possible to design the mechanical properties of the entire sandwich system, according to the RoM. Thus, as an example, with a high ratio of polymer the yield and ultimate tensile stresses (YS and UTS) as well as the Young's modulus (E) can be reduced, in order to reach properties comparable to that of the cortical bone[50,51]. Indeed, considering that the chosen Ti sheet and PMMA foil have a Young's modulus equal to (108 ± 7) GPa and (2.0 ± 0.1) GPa, two combinations of the Ti and PMMA thicknesses required to get a Ti/PMMA/Ti sandwich possessing a stiffness of about 32 GPa and an UTS of 162 MPa were suggested. Firstly, a symmetric structure (Ti/PMMA/Ti[*1] in **Table 2**), composed of two Ti sheets 0.2 mm thick and a PMMA foil 1.0 mm thick (corresponding to a PMMA volume fraction equal to 0.71). Secondly, by maintaining the same PMMA volume fraction, an asymmetric Ti/PMMA/Ti combination could be obtained using two

Ti sheets 0.2 and 0.4 mm thick and a PMMA core of 1.5 (Ti/PMMA/Ti[*2] in **Table 2**). This may result in a decrease of the bio-mechanical impairment existing between the bone and the implant.

### 3.6 Forming properties of Ti/PMMA/Ti sandwiches

The capability of shaping Ti/PMMA/Ti sandwiches was investigated performing bending, Erichsen and deep-drawing tests. For this purpose, both, symmetric and asymmetric Ti/PMMA/Ti structures were analysed.

#### 3.6.1 Three-point bending test

The bending properties of the TI/PMMA/Ti sandwiches were investigated performing three-point bending tests using punch sizes of 3 mm and 6 mm in diameter. As reported in **Figure 9a**, with a 6 mm punch all the tested samples (dashed lines) exhibited neither cracking nor delamination or interlaminar shearing at the sample edges up to a bending angle of 180°. Besides, the observed Ti/PMMA good adhesion, the ductility of the PMMA core was enough to accomplish cracking-free bending operation in all the sandwich structures (**Figure 9b**). The bending force–displacement curve for the asymmetric sandwich (0.4/0.5/0.2, black, dashed line in **Figure 9a**) is located between the two symmetric ones, i.e. 0.4/0.5/0.4 and 0.2/0.5/0.2. The punch was set in contact with the thinner Ti sheet, so the thicker (outer) layer could withstand a higher bending load. As expected, the bending tests carried-out with the smaller punch (diameter of 3 mm) on the symmetric sandwich combinations (i.e. 0.2/0.5/0.2 and 0.4/0.5/0.4) result in an increase of the bending forces for both combinations tested (light blue and red solid lines in **Figure 9a**, respectively).

Moreover, the sandwich combination built-up using the thinner Ti sheets (i.e. the 0.2/0.5/0.2 sandwich), bent with 3the 3 mm punch showed a significant decrease of the forming limit (solid

red line in **Figure 9a**). As depicted in **Figure 9a**, cracking (highlighted in **Figure 9c**) took place at a punch displacement of approx.16 mm, corresponding to a bending angle of approx. 80°.

The previous bending results can be further explained by analysing the strain field on the surface of the bent Ti samples. **Figure 10** shows the average value of the maximum major strain determined from the middle part of the bent samples shown in **Figure 11**. As expected, with the smaller punch size (3 mm, the solid lines) higher strain values resulted leading to earlier failure by cracking at about 80° in case of the thinner Ti sheet (0.2 mm).

Additionally, the strain levels, using the 6 mm punch, are less, even at higher bending angles, because of the reduced load on the outside of the sheet. The springback ratios (K) of the Ti/PMMA/Ti sandwiches in correlation with the skin/core thickness and the bending angles (45°, 90° and 135°) using the 3 mm and 6 mm punch diameters are shown in **Figure 12**.

Due to the high elastic / low plastic strain fraction existing at this angle for the first bending step (45°) lower K-values – higher springback angles - for all the sandwich results were observed. For the same sandwich sheets with the larger bending punch diameter, lower K-values resulted, too, which is in accordance with the fundamentals of springback properties (as shown in (1)) Furthermore, the asymmetric sandwich (0.4/0.5/0.2*) shows an intermediate K-value progress with the bending angle, located between the two symmetric ones, i.e. the 0.2/0.5/0.2 and 0.4/0.5/0.4. It can be stated, that bending of the sandwich sheets is in good agreement to the guidelines recommended for monolithic sheet metals, where the radius of the bending punch (r) is suggested to be twice the sheet thickness (t), i.e. $r \geq 2t$. Safe bending process can be achieved with a ratio of the punch radius R to the materials thickness of 3 (R/t >3). For high strength materials, R > 5t may be required [51].

### 3.6.2 Deep drawing

Moreover, for analysing the possibilities of shaping more complex components, deep drawing and Erichsen tests were performed. Due to the brittle behaviour of the PMMA (see **Figure 8**), the pure PMMA foil failed earlier at a punch displacement of only ~6 mm (see violet line in **Figure 13a** and **Figure 13b**).

Whereas, all the Ti/PMMA/Ti sandwich combinations (0.4/0.5/0.4 (black), 0.4/0.5/0.2 (red), 0.4/0.5/0.2 (green) in **Figure 13a**) were completely drawn without visual cracking of the Ti skin sheets (see **Figure 13c** and **Figure 13d** in the particular case of a 0.2/0.5/0.2 Ti/PMMA/Ti structure), due to the good forming behaviour of the latter one (blue line in **Figure 13a**). Nevertheless, in correspondence of a 6 mm punch displacement, a small decay of the force was observed, possibly indicating cracking of the polymer core. As no delamination occurred, the cracking of the polymer core was ignored with respect to the overall drawing behaviour of the whole sandwich. The drawing properties of the investigated sandwich combination are summarized in **Table 3**.

### 3.6.3 Erichsen tests

The cracking limit of the sandwich sheet (0.2/0.5/0.2, light blue curves in **Figure 14a**) is the same as for the Ti sheet (red curves in **Figure 14a**); however – as expected – the force of the sandwich is twice that of the pure Ti sheet. Although the PMMA foils (black curves) show a higher Erichsen index IE of 10 mm compared to the sandwich sheet and the Ti one, the failure mechanism is totally different exhibiting clearly a brittle cracking mechanism (**Figure 14b-d**). Thus, we can state that the deformation behaviour of the investigated sandwiches is good and

sufficient for a complex shaping. The failure of the PMMA foil is delayed by the supporting effect of the Ti sheets. Moreover, the cracking of the polymer can be avoided or delayed by processing under elevated temperatures or using a more ductile PMMA derivate.

## 4. Conclusions

Surface-confined PMMA chains were successfully grown on large Ti substrates (up to DIN A6 size) through SI-ATRP coupled with a "grafting from" method using phosphonic acids as coupling agents to ensure the metal-polymer covalent bonding. They were used as adhesive layers for the fabrication of biocompatible resin-free sandwich materials produced by hot-pressing. In particular, tethered PMMA chains were used to replace the epoxy resin - usually employed in sandwich materials to stick the polymer core onto the metal skin sheets - and ensure the bonding through the formation of entanglements caused by the interpenetration of the tethered PMMA chains into those of the PMMA core. Ti/PMMA/Ti sandwiches were processed demonstrating that, for the sandwich production, tethered polymer chains can replace epoxy-resin. In this way, the optimum Ti/PMMA/Ti sandwiches hot-pressing parameters (temperature, time and pressure), delivering the highest Ti/PMMA adhesion, were developed using an optimal factorial experimental plan defined by the design of experiments method. With the optimum conditions (180°, 90 min and 0.2 MPa), a high bonding strength (pull-off strength higher than 20 MPa and a shear resistance of 10 MPa) and good forming properties could be achieved. The mechanical properties determined by tensile testing showed that the failure of the sandwiches mainly depends on the failure strain of the Ti skin sheets; whereas, the brittle failure nature of the PMMA did not remarkably influence the failure strain of the sandwich. Additionally, the rule of mixture was verified with the obtained stiffness- and strength-related properties (E, YS, UTS and

ER10). Applying this rule, two sandwich combinations (symmetric and asymmetric) possessing mechanical properties - especially Young's modulus - close to that of the cortical bone were proposed. Three-point bending and deep-drawing tests were performed to analyse the forming behaviour. In particular, despite the low ductility of the PMMA core, delamination-free bending operation up to 180° were achieved without cracking of the Ti/PMMA/Ti sandwiches made of thicker Ti skin sheets (0.4 mm) for both bending punches (3 mm and 6 mm in diameter). However, for the smaller bending punch the bending angle was limited to 80° if thinner Ti skin sheets (0.2 mm) were used. Furthermore, Ti/PMMA/Ti could be completely deep-drawn without visual cracking of the Ti skin sheets, thanks to the good forming behaviour of the metal. The same behaviour could be stated for the Erichsen test, where the brittle nature of PMMA has no negative influence on the forming limits or even on the Ti/PMMA interface quality, indeed no delamination took place.

**Supplementary Information**

The following additional analyses are included: *(i)* characterization of the grafted-Ti surfaces after 3h and 24h; *(ii)* Characterization of the PMMA melting and glass transition temperatures; *(iii)* Morphological characterization of A6-sized PMMA-coated Ti samples.

AUTHOR INFORMATION

**Corresponding Author**

* melania.reggente@epfl.ch

* heinz.palkowski@tu-clausthal.de

**Acknowledgements**

We gratefully acknowledge the financial support provided by the German Research Foundation: DFG, grant no. PA 837/44-1, by IDEX Université of Strasbourg as well as Friedrich Gustav Theis Kaltwalzwerke GmbH for supplying us with the Ti sheets.

**REFERENCES**

[1] S. Aydin, B. Kucukyuruk, B. s, S. Aydin, and G. Z. Sanus, "Cranioplasty: review of materials and techniques," Journal of Neurosciences in Rural Practice, vol. 2, no. 2, p. 162, 2011.

[2] T. Origitano, R. Izquierdo, and L. B. Scannicchio, "Reconstructing complex cranial defects with a preformed cranial prosthesis," Skull Base Surgery, vol. 5, no. 02, pp. 109–116, 1995.

[3] B. Lethaus, Y. Safi, M. ter Laak-Poort, A. Kloss-Brandstätter, F. Banki, C. Robbenmenke, U. Steinseifer, and P. Kessler, "Cranioplasty with customized titanium and PEEK implants in a mechanical stress model," Journal of Neurotrauma, vol. 29, no. 6, pp. 1077–1083, 2012.

[4] A. Thien, N. K. King, B. T. Ang, E. Wang, and I. Ng, "Comparison of polyetheretherketone and titanium cranioplasty after decompressive craniectomy," World neurosurgery, vol. 83, no. 2, pp. 176–180, 2015.

[5] B. L. Eppley, L. Hollier, and S. Stal, "Hydroxyapatite cranioplasty: 2. clinical experience with a new quick-setting material," Journal of Craniofacial Surgery, vol. 14, no. 2, pp. 209–214, 2003.

[6] Y. Ducic, "Titanium mesh and hydroxyapatite cement cranioplasty: a report of 20 cases," Journal of Oral and Maxillofacial Surgery, vol. 60, no. 3, pp. 272–276, 2002.

[7] P. D. Costantino, C. D. Friedman, K. Jones, L. C. Chow, and G. A. Sisson, “Experimental hydroxyapatite cement cranioplasty.,” Plastic and Reconstructive Surgery, vol. 90, no. 2, pp. 174–85 1992.

[8] M. Cabraja, M. Klein, and T.-N. Lehmann, “Long-term results following titanium cranioplasty of large skull defects,” Neurosurgical Focus, vol. 26, no. 6, p. E10, 2009.

[9] T.P. Queiroz, R.S., de Molon, F.Á. Souza, R. Margonar, A.H.A. Thomazini, A.C. Guastaldi, E. Hochuli-Vieira, “In vivo evaluation of cp Ti implants with modified surfaces by laser beam with and without hydroxyapatite chemical deposition and without and with thermal treatment: topographic characterization and histomorphometric analysis in rabbits”, Clinical oral investigations, vol. 21, no. 2, pp. 685−699, 2017.

[10] C. Debry, N.E. Vrana, A. Dupret-Bories, Implantation of an Artificial Larynx after Total Laryngectomy. N. Engl. J. Med. 2017, 376, 97−98.

[11] A. Carradò, F. Perrin-Schmitt, Q.V. Le, M. Giraudel, C. Fischer, G. Koenig, G. Koenig, L. Jacomine, L. Behr, A. Chalom, L. Fiette, A. Morlet, G. Pourroy, “Nanoporous hydroxyapatite/sodium titanate bilayer on titanium implants for improved osteointegration”, Dental Materials, vol. 33, no. 3, pp. 321−332, 2017.

[12] L.A. Dobrzański, A.D. Dobrzańska-Danikiewicz, A. Achtelik-Franczak, L.B. Dobrzański, M. Szindler, T.G. Gaweł, “Porous selective laser melted Ti and $Ti_6Al_4V$ materials for medical applications. In Powder Metallurgy-Fundamentals and Case Studies. InTech, 2017.

[13] S. Mueller, B. Hohlweg-Majert, R. Buergers, T. Steiner, T.E. Reichert, K.D. Wolff, M. Gosau, “The functional and aesthetic reconstruction of midfacial and orbital defects by

combining free flap transfer and craniofacial prosthesis", Clinical oral investigations, vol. 19, no. 2, pp. 413–419, 2015.

[14] A.L. Jardini, M.A. Larosa, R. Maciel Filho, C.A. de Carvalho Zavaglia, L.F. Bernardes, C.S. Lambert, D.R. Calderoni, P. Kharmandayan, "Cranial reconstruction: 3D biomodel and custom-built implant created using additive manufacturing", Journal of Cranio-Maxillo-Facial Surgery, vol. 42, no. 8, pp. 1877–1884, 2014.

[15] H. Rotaru, R. Schumacher, S.G. Kim, C. Dinu, "Selective laser melted titanium implants: a new technique for the reconstruction of extensive zygomatic complex defects", Maxillofacial plastic and reconstructive surgery, vol. 37, no. 1, pp. 1, 2015.

[16] G.J. Huang, S. Zhong, S.M. Susarla, E.W. Swanson, J. Huang, C.R. Gordon, "Craniofacial reconstruction with poly (methyl methacrylate) customized cranial implants" Journal of Craniofacial Surgery, vol. 26, no. 1, pp. 64–70, 2015.

[17] A. Ridwan-Pramana, P. Marcián, L. Borák, N. Narra, T. Forouzanfar, J. Wolff, "Structural and mechanical implications of PMMA implant shape and interface geometry in cranioplasty–A finite element study", Journal of Cranio-Maxillo-Facial Surgery, vol. 44, no. 1, pp. 34–44, 2016.

[18] M. Ridzwan, S. Shuib, A. Hassan, A. Shokri, and M. M. Ibrahim, "Problem of stress shielding and improvement to the hip implant designs: a review," Journal of Medical Science, vol. 7, no. 3, pp. 460–467, 2007.

[19] A. J. Ruys, Biomimetic biomaterials: structure and applications. Elsevier, 2013.

[20] B. Harris, “A perspective view of composite materials development,” Materials & Design, vol. 12, no. 5, pp. 259–272, 1991.

[21] R. F. Landel and L. E. Nielsen, Mechanical properties of polymers and composites. CRC Press, 1993.

[22] O. T. Thomsen, E. Bozhevolnaya, and A. Lyckegaard, Sandwich Structures 7: Advancing with Sandwich Structures and Materials: Proceedings of the 7th International Conference on Sandwich Structures, Aalborg University, Aalborg, Denmark, 29-31 August 2005. Springer Science & Business Media, 2006.

[23] M. Harhash, A. Carradò, and H. Palkowski, “Lightweight titanium/polymer/titanium sandwich sheet for technical and biomedical application,” Materialwissenschaft und Werkstofftechnik, vol. 45, no. 12, pp. 1084–1091, 2014.

[24] Y. S. Chen, T. J. Hsu, S. I. Chen, “Vibration damping characteristics of laminated steel sheet”, Metallurgical transactions A, vol. 22, no. 3, pp. 653−656, 1991.

[25] E. Bernd, J. Buhl, “Metal Forming of Vibration-Damping Composite Sheets”, Steel Research International, vol. 82, no. 6, pp. 626−631, 2011.

[26] G. D. Parfitt, Adsorption from solution at the solid/liquid interface. Academic Pr, 1983.

[27] L. Librescu and T. Hause, “Recent developments in the modeling and behavior of advanced sandwich constructions: a survey,” Composite structures, vol. 48, no. 1, pp. 1–17, 2000.

[28] O. A. Sokolova, A. Carradò, and H. Palkowski, “Metal–polymer–metal sandwiches with local metal reinforcements: A study on formability by deep drawing and bending,” Composite Structures, vol. 94, no. 1, pp. 1–7, 2011.

[29] E. L. Kostoryz, P. Y. Tong, C. C. Chappelow, J. D. Eick, A. G. Glaros, D. M. Yourtee, “In vitro cytotoxicity of solid epoxy-based dental resins and their components” Dental Materials, vol. 15, no. 5, pp. 363−373, 1999.

[30] Y. Fujimoto, Y. Kobayashi, M. Yamaguchi, “Delamination of abluminal polymer of biolimus-eluting stent. JACC: Cardiovascular Interventions”,vol. 5, no. 3, pp. e5-e6, 2012.

[31] C. Sun, F. Zhou, L. Shi, B. Yu, P. Gao, J. Zhang, and W. Liu, “Tribological properties of chemically bonded polyimide films on silicon with polyglycidyl methacrylate brush as adhesive layer,” Applied Surface Science, vol. 253, no. 4, pp. 1729–1735, 2006.

[32] Y. Shaulov, R. Okner, Y. Levi, N. Tal, V. Gutkin, D. Mandler, A. J. Domb, “Poly (methyl methacrylate) grafting onto stainless steel surfaces: application to drug-eluting stents”. ACS applied materials & interfaces, vol. 1, no. 11, pp. 2519-2528, 2009.

[33] K. Shimizu, K. Malmos, A. H. Holm, S. U. Pedersen, K. Daasbjerg, and M. Hinge, “Improved adhesion between PMMA and stainless steel modified with PMMA brushes,” ACS Applied Materials & Interfaces, vol. 6, no. 23, pp. 21308–21315, 2014.

[34] K. Shimizu, K. Malmos, S. A. Spiegelhauer, J. Hinke, A. H. Holm, S. U. Pedersen, K. Daasbjerg, and M. Hinge, “Durability of peek adhesive to stainless steel modified with aryldiazonium salts,” International Journal of Adhesion and Adhesives, vol. 51, pp. 1–12, 2014.

[35] O. Alageel, M.-N. Abdallah, Z. Y. Luo, J. Del-Rio-Highsmith, M. Cerruti, and F. Tamimi, "Bonding metals to poly (methyl methacrylate) using aryldiazonium salts," Dental Materials, vol. 31, no. 2, pp. 105–

114, 2015.

[36] M. Aubouy, G. Fredrickson, P. Pincus, and E. Raphaeel, "End-tethered chains in polymeric matrixes," Macromolecules, vol. 28, no. 8, pp. 2979– 2981, 1995.

[37] W. S. Gutowski, S. Li, C. Filippou, P. Hoobin, and S. Petinakis, "Interface/ interphase engineering of polymers for adhesion enhancement: Part ii. theoretical and technological aspects of surface-engineered interphaseinterface systems for adhesion enhancement," The Journal of Adhesion, vol. 79, no. 5, pp. 483–519, 2003.

[38] S. W. Sides, G. S. Grest, M. J. Stevens, and S. J. Plimpton, "Effect of end-tethered polymers on surface adhesion of glassy polymers," Journal of Polymer Science Part B: Polymer Physics, vol. 42, no. 2, pp. 199−208, 2004.

[39] E. Raphael and P. De Gennes, "Rubber-rubber adhesion with connector molecules," The Journal of Physical Chemistry, vol. 96, no. 10, pp. 4002– 4007, 1992.

[40] K. Kunz and M. Stamm, "Initial stages of interdiffusion of PMMA across an interface," Macromolecules, vol. 29, no. 7, pp. 2548–2554, 1996.

[41] R. Schnell, M. Stamm, and C. Creton, "Direct correlation between interfacial width and adhesion in glassy polymers," Macromolecules, vol. 31, no. 7, pp. 2284–2292, 1998

[42] C. Gay, "Wetting of a polymer brush by a chemically identical polymer melt," Macromolecules, vol. 30, no. 19, pp. 5939–5943, 1997.

[43] C. F. Laub and J. T. Koberstein, “Effect of brush polydispersity on the interphase between end-grafted brushes and polymeric matrixes,” Macromolecules, vol. 27, no. 18, pp. 5016–5023, 1994.

[44] J. E. Friis, K. Brøns, Z. Salmi, K. Shimizu, G. Subbiahdoss, A. H. Holm, O. Santos, S. U. Pedersen, R. L. Meyer, K. Daasbjerg, et al., “Hydrophilic polymer brush layers on stainless steel using multilayered ATRP initiator layer,” ACS Applied Materials & Interfaces, vol. 8, no. 44, pp. 30616–30627, 2016.

[45]M. Reggente, P. Masson, C. Dollinger, H. Palkowski, S. Zafeiratos, L. Jacomine, D. Passeri, M. Rossi, N.E. Vrana, G. Pourroy, A. Carradò, “A novel alkali-activation of titanium substrates to grow thick and covalently bound PMMA layers” ACS applied materials & interfaces, vol. 10, pp. 5967−5977, 2018.

[46] J. S. Wang, K. Matyjaszewski, “Controlled/“living” radical polymerization. Atom transfer radical polymerization in the presence of transition-metal complexes”, Journal of the American Chemical Society,

vol. 117, no. 20, pp. 5614–5615, 1995.

[47] G. Guerrero, P.H. Mutin, A. Vioux, “Anchoring of Phosphonate and Phosphinate Coupling Molecules on Titania Particles” Chemistry of Materials, vol. 13, pp. 4367−4373, 2001.

[48] V. Vergnat, G. Pourroy, P. Masson, P., “Enhancement of styrene conversion in organic/inorganic hybrid materials by using malononitrile in controlled radical polymerization”, Polymer International, vol. 62, no. 6, pp. 878−883, 2013.

[49] M. Reggente, M. Natali, D. Passeri, M. Lucci, I. Davoli, G. Pourroy, G., P. Masson, H. Palkowski, U. Hangen, A.Carradò, M. Rossi "Multiscale mechanical characterization of hybrid Ti/PMMA layered materials" Colloids and Surfaces A: Physicochemical and Engineering Aspects, vol. 532, pp. 244−251, 2017.

[50] Tekiner Z, "An experimental study on the examination of springback of sheet metals with several thicknesses and properties in bending dies," Journal of Materials Processing Technology, vol. 145, no. 1, pp. 109-117, 2004.

[51] Marciniak Z, Duncan JL, Hu SJ, "Mechanics of sheet metal forming," 2nd ed. Oxford, Boston: Butterworth-Heinemann, 2002.

[52] J.Y. Rho, R. B. Ashman, and C. H. Turner, "Young's modulus of trabecular and cortical bone material: ultrasonic and microtensile measurements," Journal of Biomechanics, vol. 26, no. 2, pp. 111–119, 1993.

[53] P.K. Zysset, X. E. Guo, C. E. Hoffler, K. E. Moore, and S. A. Goldstein, "Elastic modulus and hardness of cortical and trabecular bone lamellae measured by nanoindentation in the human femur," Journal of Biomechanics, vol. 32, no. 10, pp. 1005–1012, 199.

# Figures

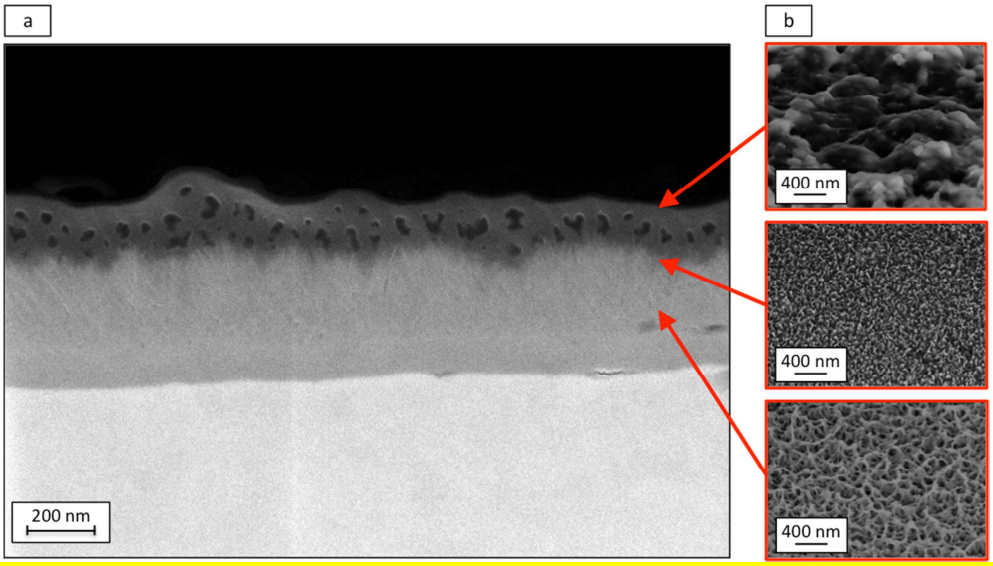


**Figure 1:** a) SEM image of a PMMA-coated Ti cross-section, (b) the porous structure, typical for the alkali-activated Ti (bottom); the more compact $C_7H_{14}O_5PBr$ modified surface (middle); the structure of the grown PMMA layer (top).

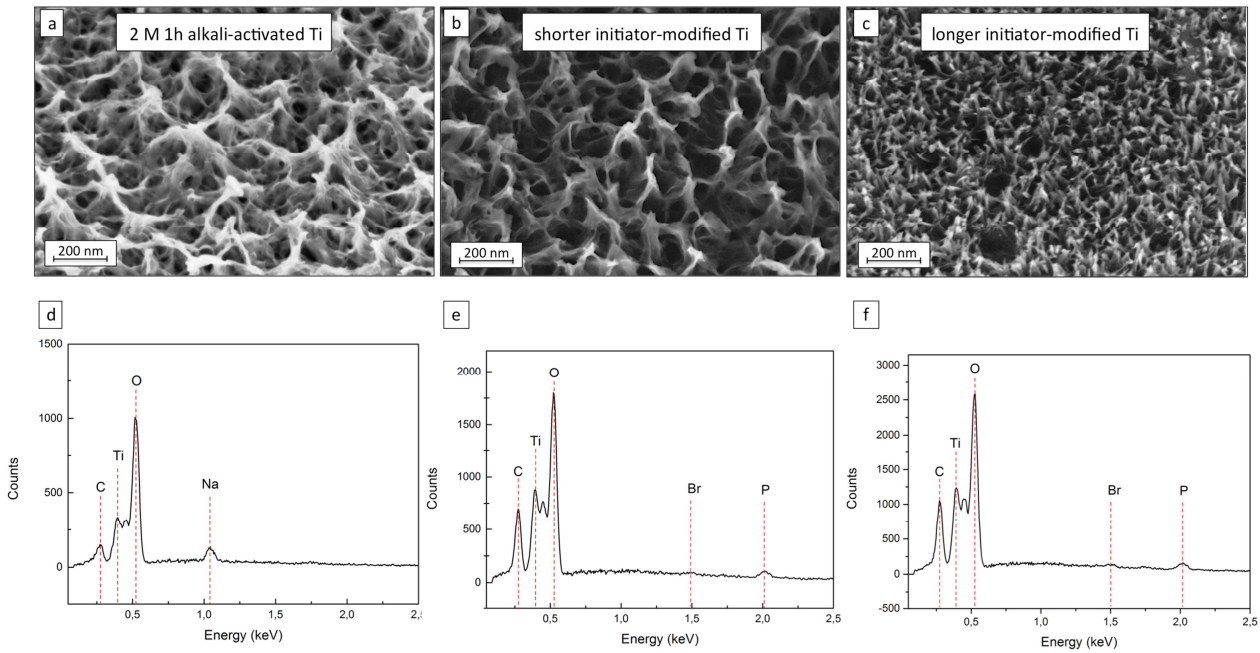


**Figure 2:** SEM micrographs of a: a) alkali-activated surface; b) $C_7H_{14}O_5PBr$ initiator modified surface and c) $C_{15}H_{30}O_5PBr$ initiator modified surface. EDX spectra of: d) alkali-activated surface; e) $C_7H_{14}O_5PBr$ initiator modified surface and f) $C_{15}H_{30}O_5PBr$ initiator modified surface.

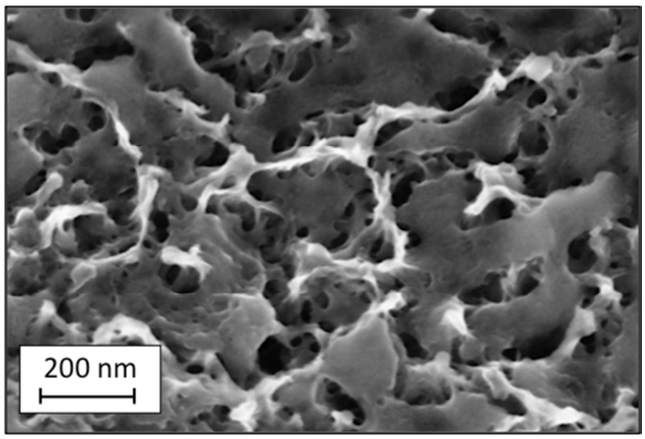


**Figure 3**: SEM micrograph of the PMMA layer grown starting from a short-initiator ($C_7H_{14}O_5PBr$) modified Ti surface.

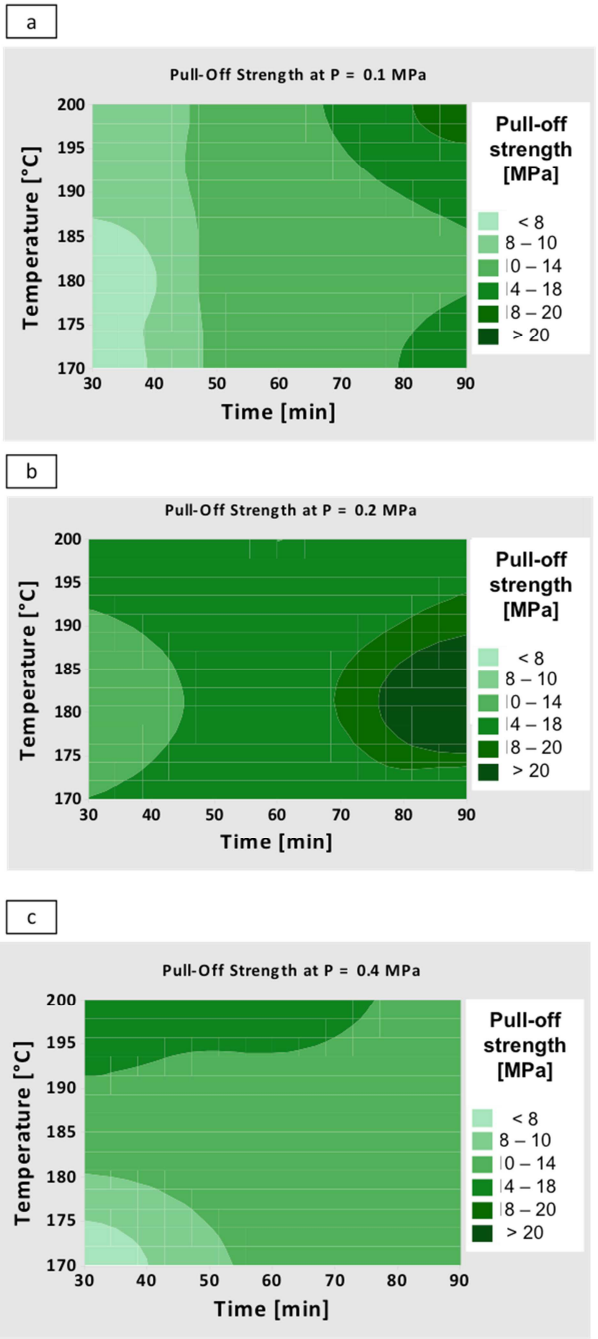


**Figure 4**: Contour charts showing the mutual effect of the hot-pressing time and temperature at constant pressures of 0.1 MPa (a), 0.2 MPa (b) and 0.4 MPa (c) on the Ti/PMMA/Ti pull-off strength.

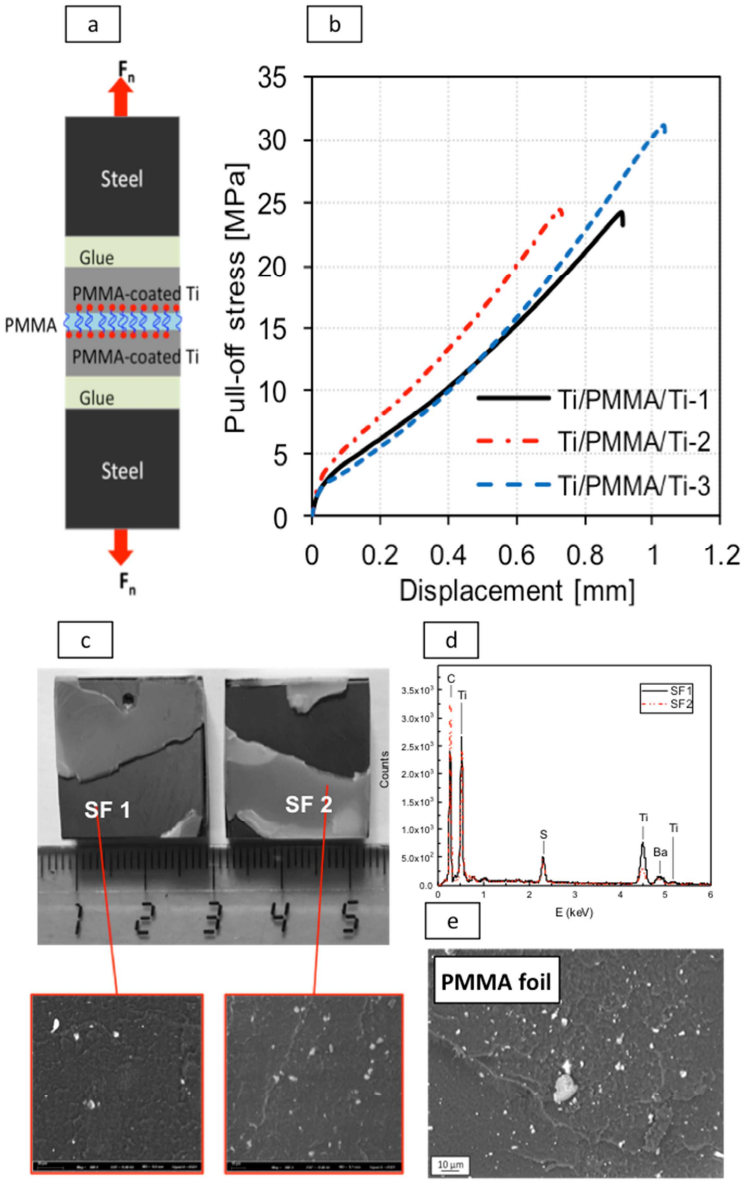


**Figure 5**: a) schematization of the pull-off test set-up. The external part of the sandwich was fixed on a steel support required to insert the sample in the universal testing machine. b) Stress-strain curves obtained performing the pull-off tests of three Ti/PMMA/Ti sandwiches produced with the identified optimum conditions. c) Fracture surfaces of a representative Ti/PMMA/Ti sandwich after pull-off test together with two SEM micrographs recorded on both the sides of the fracture surfaces. d) EDX spectra a Ti/PMMMA/Ti sandwich surface fracture (black line corresponds to point SF1 and the red

one to SF2). e) SEM micrograph of the PMMA foil used as core material (white spots correspond to $BaSO_4$ fillers).

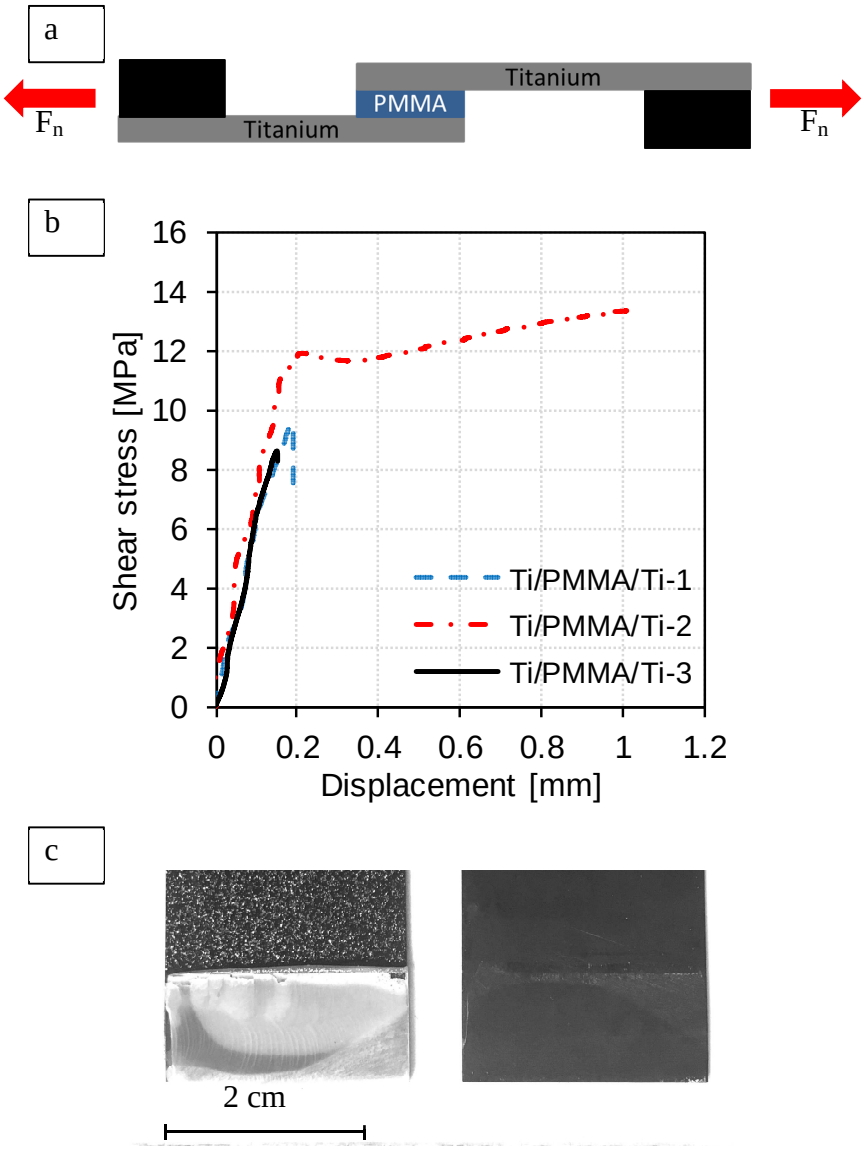


**Figure 6**: a) Schematization of the sample geometry used to perform shear tests. b) Shear stress-displacement for three sandwich samples (Ti/PMMA/Ti: 0.4/0.5/0.4) produced using the

optimum conditions (T = 180°C, t = 90 min, p = 0.2 MPa). c) Representative fracture surfaces after shear tests.

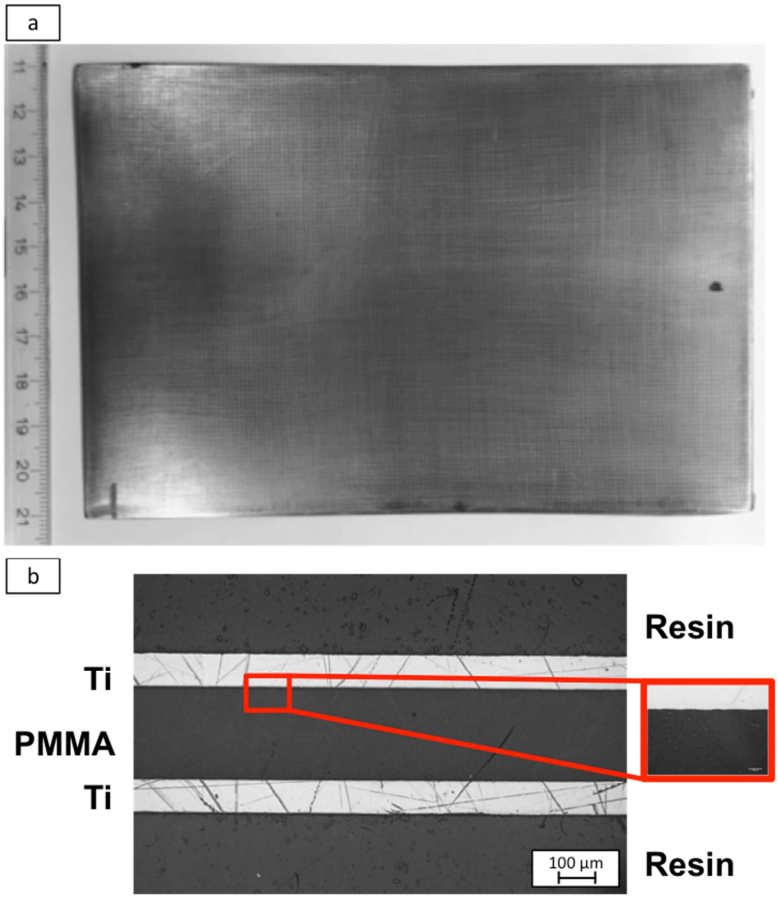


**Figure 7:** A6-sized Ti/PMMA/Ti sandwich (a) and an optical micrograph of its cross-section (b).

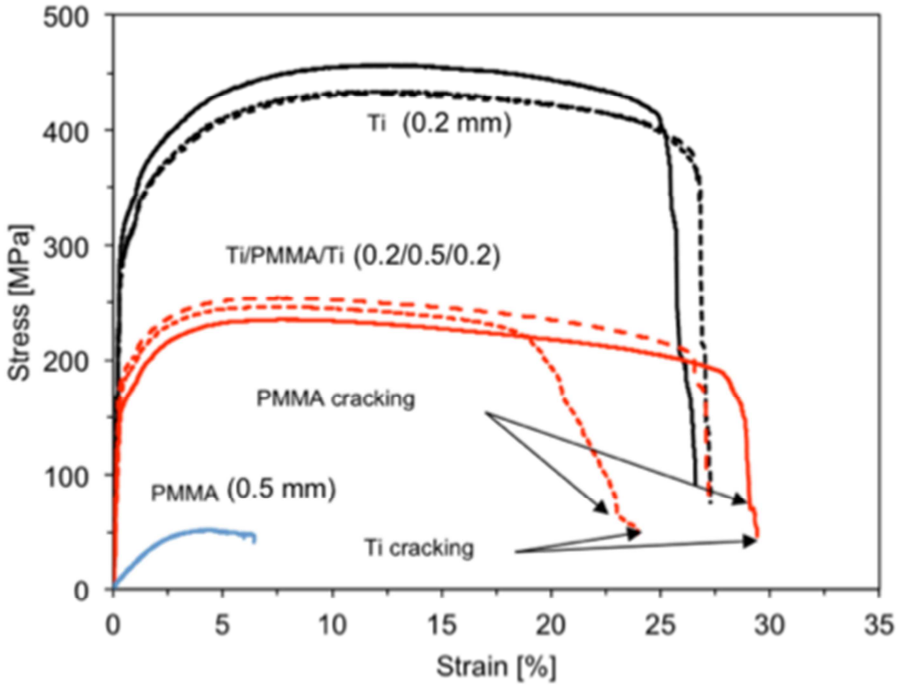


**Figure 8**: Stress-strain curves of Ti (black curves, upper three ones), PMMA (blue curve, lower one) as well as Ti/PMMA/Ti (red curves, medium three ones) samples obtained performing tensile tests.

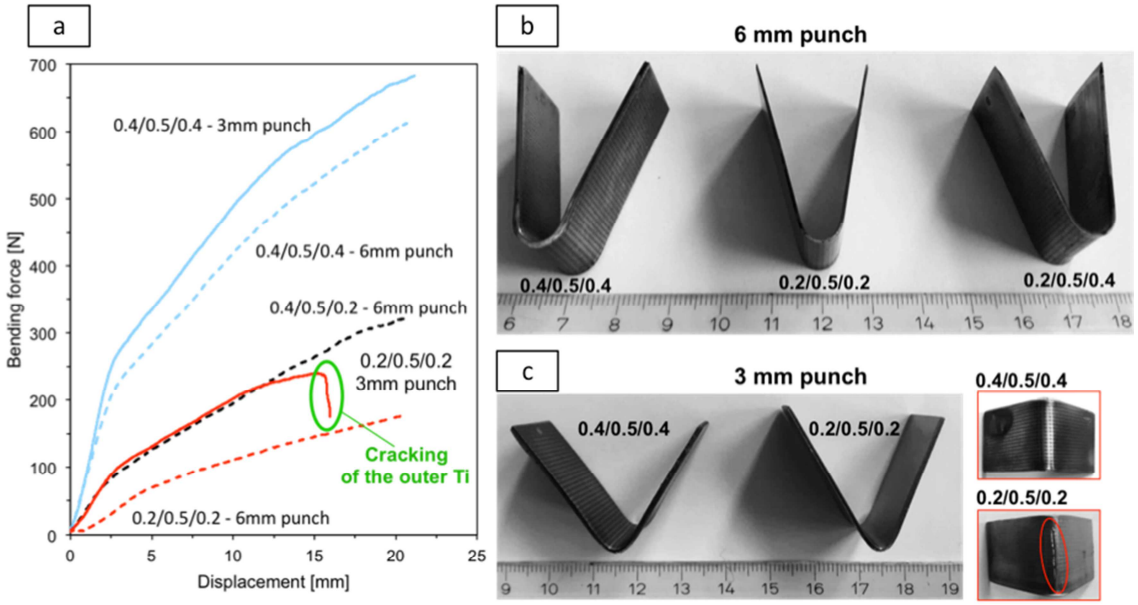


**Figure 9:** a) Bending force – displacement curves for different thickness combinations and punch diameters of 3 mm and 6 mm. b) Ti/PMMA/Ti sandwiches bent up to 180° with a 6 mm punch. c) Ti/PMMA/Ti sandwiches bent up to about 80° with a 3 mm punch.

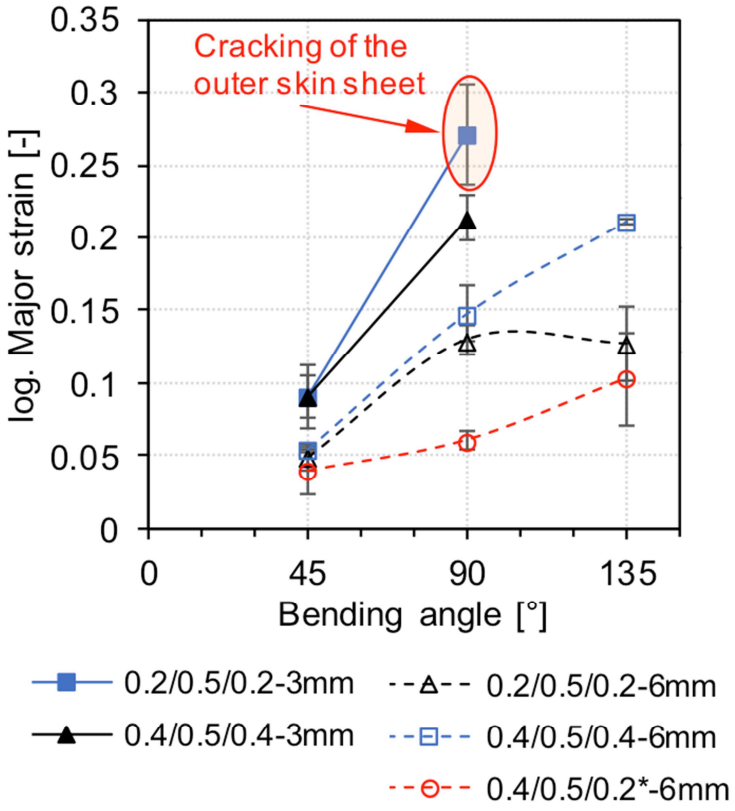


**Figure 10**: Average maximum major strains of the bent samples in correlation with the punch size, bending angle and skin/core thickness configurations.

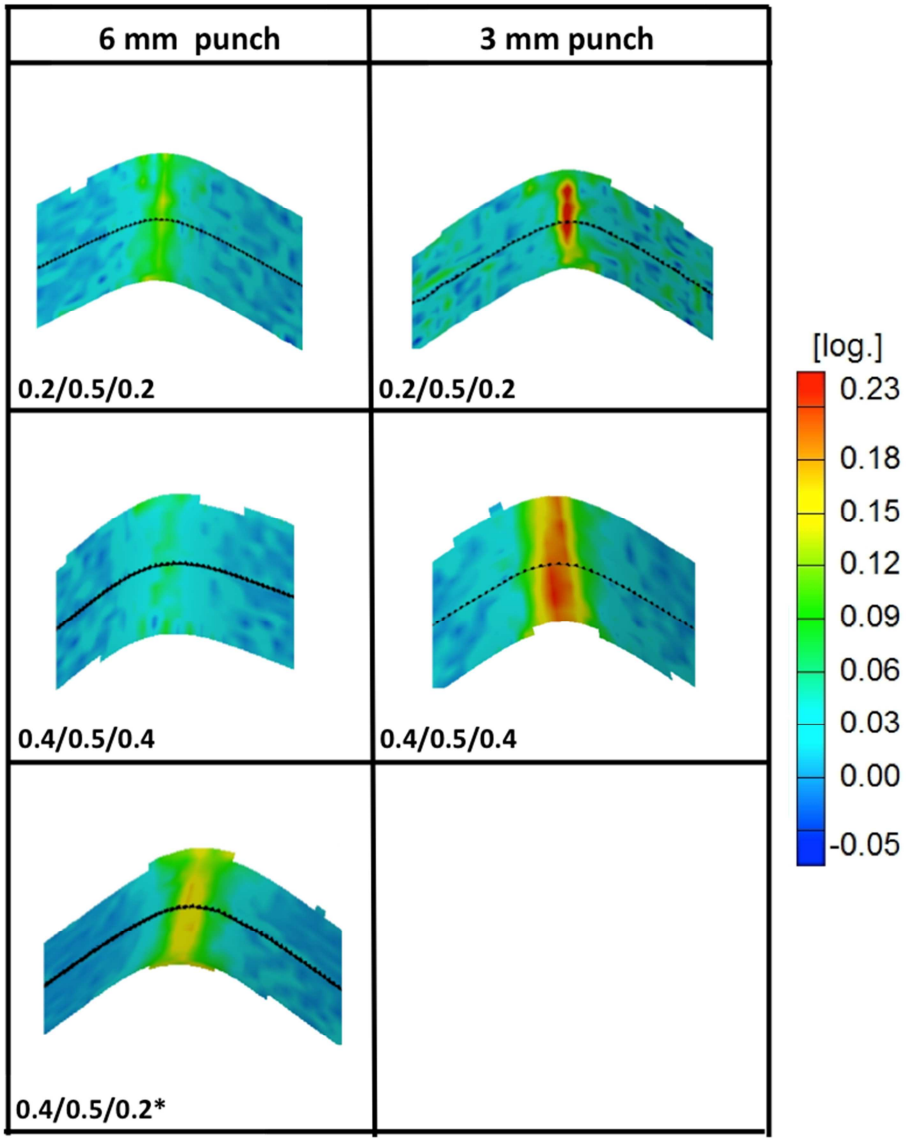


**Figure 11:** Photogrammetric images of the bent samples at 90°. *: indicating the Ti skin sheet in contact with the punch during the bending test.

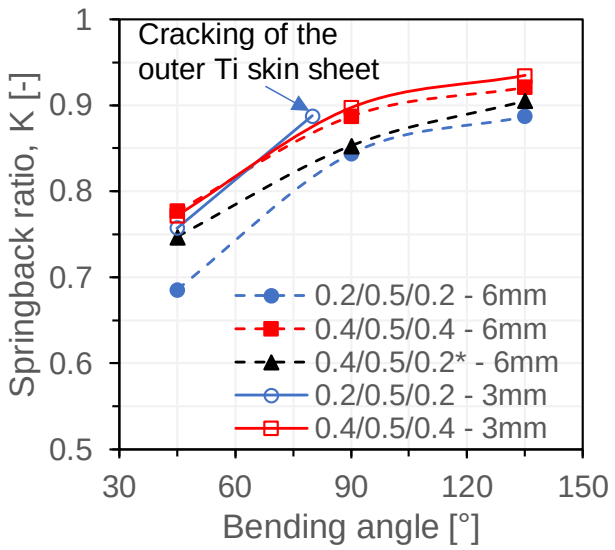


**Figure 12:** Springback ratio of the Ti/PMMA/Ti sandwiches in correlation with the skin/core thickness and the bending angles (45°, 90° and 135°). Punch diameters: 3 mm (solid lines), 6 mm (dotted lines).

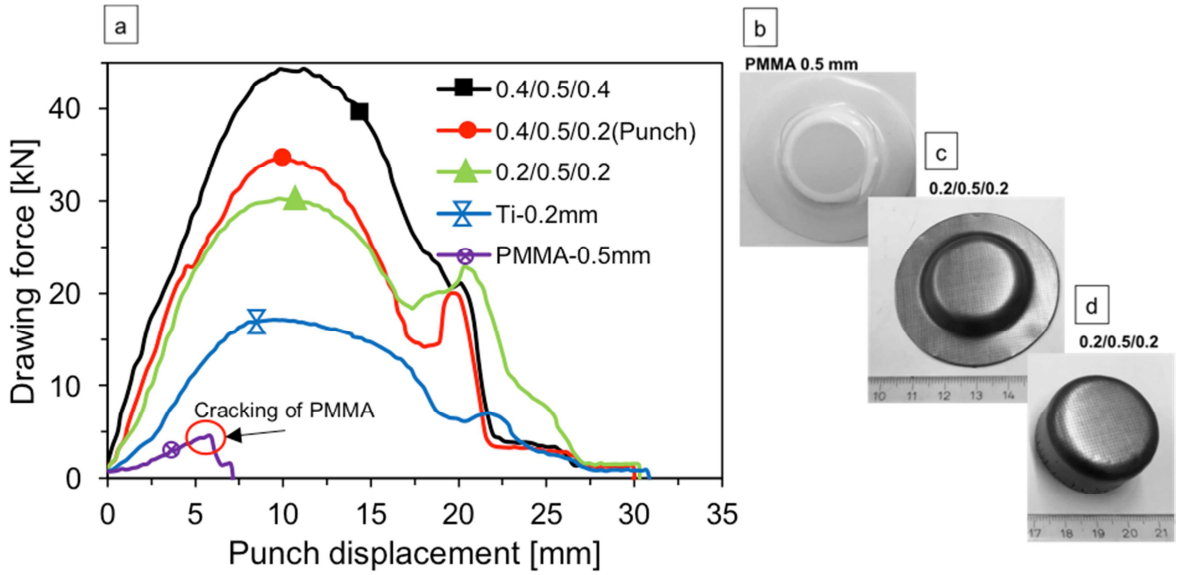


**Figure 13:** a) Drawing force-punch displacement curves for the tested combinations ($ß_0 = 1,8$), b) Cracking of the PMMA foil 0.5 mm thick, drawn up to a displacement of 6 mm. c) 0.2/0.5/0.2 Ti/PMMA/Ti, drawn up to a displacement of 6 mm. d) 0.2/0.5/0.2 Ti/PMMA/Ti completely drawn.

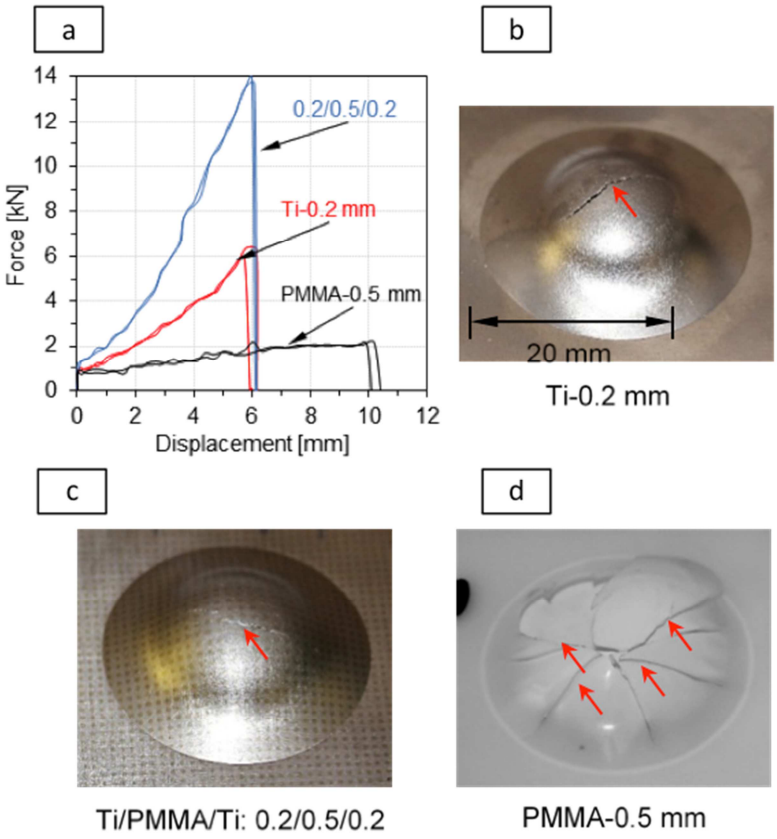


**Figure 14:** a) Drawing force-punch displacement curves for the tested materials according to Erichsen test and b) the cracked samples showing the central failure location (two samples/each condition were tested).

# Tables

**Table 1:** Experimental parameters used for the Ti/PMMA/Ti sandwich production – according to the DoE plan – and their corresponding adhesion strength evaluated in pull-off tests.

| Temperature [°C] | Time [min] | Pressure [MPa] | Pull-off strength [MPa] |
|---|---|---|---|
| 170 | 30 | 0.1 | 7 ± 1 |
| | | 0.4 | 7 ± 1 |
| | 60 | 0.1 | 11 ± 4 |
| | | 0.2 | 16 ± 6 |
| | 90 | 0.1 | 16 ± 7 |
| | | 0.2 | 16 ± 5 |
| | | 0.4 | 11 ± 1 |
| 180 | 30 | 0.1 | 6 ± 2 |
| | | 0.2 | 12 ± 5 |
| | 60 | 0.1 | 12 ± 2 |
| | | 0.4 | 10 ± 1 |
| | 90 | 0.2 | 24 ± 1 |
| | | 0.4 | 13 ± 3 |
| 200 | 30 | 0.1 | 9 ± 1 |
| | | 0.2 | 14 ± 1 |
| | | 0.4 | 16 ± 8 |
| | 60 | 0.2 | 14 ± 3 |
| | | 0.4 | 15 ± 5 |
| | 90 | 0.1 | 19 ± 2 |

**Table 2**: Tensile properties of the mono-materials (Ti, PMMA) and the sandwiches (Ti/PMMA/Ti) as well as theoretical values (Ti/PMMA/Ti*[1], Ti/PMMA/Ti*[2]) proposed using the RoM providing mechanical properties close to the cortical bone ($E = 15 - 30GPa$)[52,53]. Where, $f_{PMMA}$: volume fraction, YS and UTS: yield strength and ultimate tensile strength, E: Young's modulus and ER: elongation to rupture.

| Sample | Thickness [mm] | $f_{PMMA}$ [-] | E [GPa] | | UTS [MPa] | | YS [MPa] | | ER[%] |
|---|---|---|---|---|---|---|---|---|---|
| | | | Experim. | RoM | Experim. | RoM | Experim. | RoM | |
| Ti | 0.2 | 0 | 108 ± 7 | | 441 ± 14 | - | 289 ± 15 | - | 27 ± 1 |
| PMMA | 0.5 | 1.0 | 2.0 ± 0.1 | | 51 ± 1 | - | - | - | 6 ± 1 |
| Ti/PMMA/Ti | 0.9 (0.2/0.5/0.2) | 0.55 | 51 ± 3 | 55 | 245 ± 10 | 246 | 179 ± 14 | 170 | 27 ± 3 |
| Ti/PMMA/Ti*[1] | 1.4 (0.2/1.0/0.2) | 0.71 | - | 32 | - | 162 | - | 119 | 27** |
| Ti/PMMA/Ti*[2] | 2.1 (0.4/1.5/0.2) | 0.71 | - | 32 | - | 162 | - | 119 | 27** |
| *: calculated sandwich combination; **: expected, based on the strain at failure of the Ti sheet | | | | | | | | | |

**Table 3:** Deep-drawing parameters used for the monomaterials (Ti and PMMA) as well as the Ti/PMMA/Ti sandwich in addition to the obtained results. Drawing ratio, $ß_0 = 1.8$.

| Sample notation | Thickness [mm] | Blank holding force [kN] | Max. drawing force [kN] | Drawing depth [mm] |
|---|---|---|---|---|
| Ti | 0.2 | 10 | 17±2 | Drawn cup |
| PMMA | 0.5 | 8 | 5±1 | ~6 mm cracking |
| Ti/PMMA/Ti | 0.4/0.5/0.4 | 8 | 45±1 | Drawn cup:<br>• No cracking of the skin sheets<br>• Cracking of the PMMA core |
| Ti/PMMA/Ti | 0.4*/0.5/0.2 | 8 | 35±1 | |
| Ti/PMMA/Ti | 0.2/0.5/0.2 | 7 | 30±1 | |
| * Refers to the outer skin sheet (not in contact with the punch under deep drawing) | | | | |

1. Growth of grafted PMMA layers on Ti surfaces

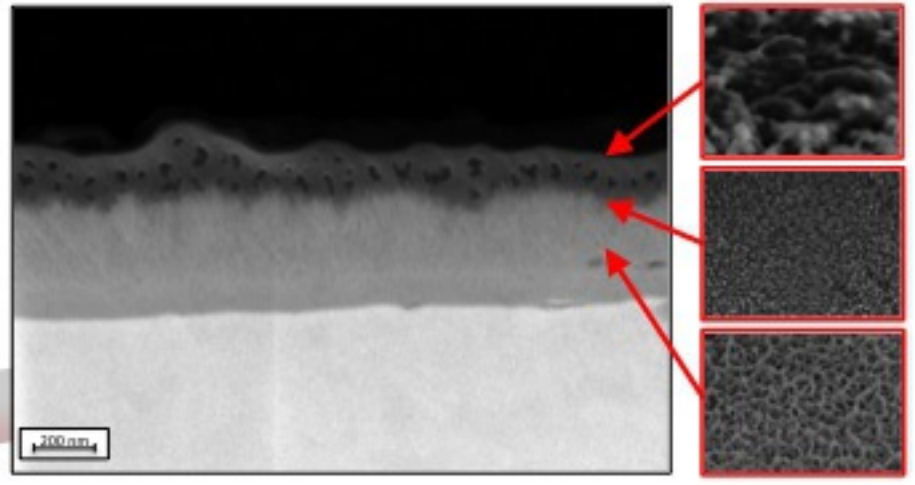


2. Biocompatible Ti/PMMA/Ti sandwich production

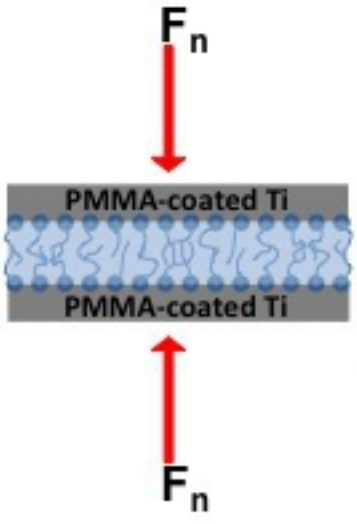


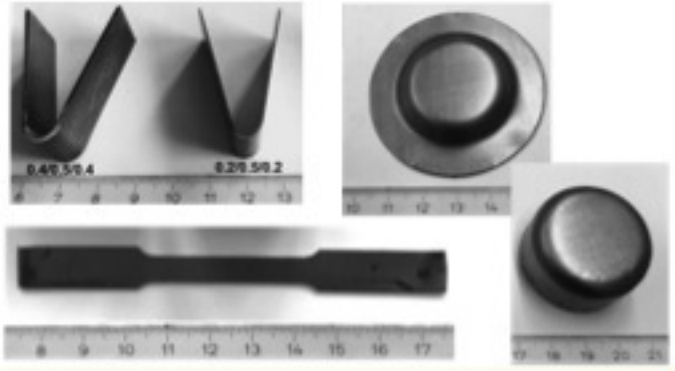

3. Mechanical testing of the bio-TI/PMMA/TI sandwiches